Fifth-Order A-WENO Finite-Difference Schemes Based on the Central-Upwind Rankine-Hugoniot Fluxes

Bao-Shan Wang*, Wai Sun Don†, Alexander Kurganov‡ and Yongle Liu §

Abstract

We construct new fifth-order alternative WENO (A-WENO) schemes for the Euler equations of gas dynamics. The new scheme is based on the central-upwind Rankine-Hugoniot (CURH) numerical flux, which has been recently proposed in [N. K. Garg, A. Kurganov and Y. Liu, J. Comput. Phys., 428 (2021)] in the context of second-order semi-discrete finite-volume methods. The CURH flux contains a smaller amount of numerical dissipation compared with the adaptive diffusion central numerical flux, which was also developed with the help of the discrete Rankine-Hugoniot conditions and used in the A-WENO scheme recently introduced in [B. S. Wang, W. S. Don, N. K. Garg and A. Kurganov, SIAM J. Sci. Comput., 42 (2020)]. As in that work, we here use the fifth-order characteristic-wise WENO-Z interpolations to evaluate the fifth-order point values required by the numerical fluxes. The resulting one- and two-dimensional schemes are tested on a number of numerical examples, which clearly demonstrate that the new schemes outperform the existing fifth-order A-WENO schemes without compromising the robustness.

Key words: A-WENO schemes; central-upwind schemes; discrete Rankine-Hugoniot conditions; numerical dissipation switch; local speeds of propagation; Euler equations of gas dynamics.

AMS subject classification: 65M06, 76M20, 65M08, 76M12, 76N15, 76L05, 35L65.

1 Introduction

This study is devoted to high-order finite-difference schemes for hyperbolic systems of conservation laws, which in the one-dimensional (1-D) case read as

$$\boldsymbol{U}_t + \boldsymbol{F}(\boldsymbol{U})_x = \boldsymbol{0}. \tag{1.1}$$

*School of Mathematical Sciences, Ocean University of China, Qingdao, 266100, China; wbs@stu.ouc.edu.cn

†School of Mathematical Sciences, Ocean University of China, Qingdao, 266100, China; donwaisun@outlook.com

‡Department of Mathematics, SUSTech International Center for Mathematics and Guangdong Provincial Key Laboratory of Computational Science and Material Design, Southern University of Science and Technology, Shenzhen, 518055, China; alexander@sustech.edu.cn

§Department of Mathematics, Southern University of Science and Technology, Shenzhen, 518055, China; liuyl2017@mail.sustech.edu.cn

Here, x and t are spatial and temporal variables, respectively, $\boldsymbol{U}(x,t) \in \mathbb{R}^N$ is a vector of conserved variables, and $\boldsymbol{F}$ is a flux function.

It is well-known that solutions of the system (1.1) may develop complicated structures including shock waves, rarefactions, and contact discontinuities even for smooth initial data. It is therefore not so easy to develop robust and highly accurate numerical methods for (1.1). Finite-volume Godunov-type schemes provide a popular framework for development of such methods; see, e.g., the monographs [6, 9, 12, 19]. Recall that in the framework of semi-discrete Godunov-type schemes, the solution is represented in terms of its cell averages, which are evolved in time with the help of the numerical fluxes, computed, in turn, using the reconstructed point values of $\boldsymbol{U}$ at the both sides of the cell interfaces. The latter point-values are computed using a global piecewise polynomial approximation, which is supposed to be made non-oscillatory with the help of nonlinear limiters. Notice that second-order schemes employ second-order piecewise linear reconstructions, while higher-order schemes have to utilize higher-degree polynomials, whose oscillations are much harder to control, especially in the multidimensional case.

Also recall that upwind numerical fluxes are computed based on either the exact or approximate solution of the (generalized) Riemann problems, which might make the resulting scheme quite complicated and computationally expensive; see, e.g., [1] and references therein. Non-oscillatory central, and especially central-upwind (CU) numerical fluxes provide one with a much simpler, more robust and yet very accurate alternative to the upwind fluxes. Unlike their upwind counterparts, CU fluxes do not employ any (generalized) Riemann problem solver, they only require the one-sided local speeds of propagation computed using upper/lower bounds on the largest/smallest eigenvalues of the Jacobian $\partial\boldsymbol{F}/\partial\boldsymbol{U}$. We refer the reader to [4, 14, 15, 17] for the derivation of the second-order CU schemes; also see the review paper [13] and references therein.

In general, CU numerical fluxes have larger amount of numerical dissipation (ND) compared with the upwind numerical fluxes. Several attempts to reduce the ND present in the CU fluxes have been made. In the recent work [4], we have utilized two different mechanisms to further reduce the ND. First, we have followed [5,10,25,30] and used discrete Rankine-Hugoniot conditions to more accurately estimate the one-sided local speeds of propagation. Second, in the two-dimensional (2-D) case, we have implemented the ND switch recently introduced in [24], and then modified in [15, 16]. The main idea of this switch is to locally reduce the influence of the acoustic wave speeds in the directions tangent to the dominating direction of the fluid flows in the neighborhoods of contact waves and shear layers. The resulting CU schemes were called in [4] central-upwind Rankine-Hugoniot (CURH) schemes.

In this paper, we incorporate the CURH numerical fluxes into the alternative WENO (A-WENO) finite-difference framework. A-WENO schemes, proposed in [11] (also, see [23]), employ standard finite-volume numerical fluxes, whose accuracy, in the context of finite-difference schemes, is limited to the second order, while a high order is achieved using the flux Taylor expansion. A-WENO schemes have been typically implemented using the simplest Rusanov (local Lax-Friedrichs) numerical flux (see [22,31]) or its lower ND extension recently proposed in [30]. Here, we use the CURH numerical flux together with the fifth-order characteristic-wise alternative WENO polynomial interpolation procedure with the Z-type weights (WENO-Z) [11,22,31], which was also used in [2, 20, 30]. We briefly describe the new A-WENO schemes in §2, and then test them in §3 on a number of challenging numerical examples for both 1-D and 2-D Euler equations of gas dynamics. We demonstrate that the new schemes outperform the fifth-order A-WENO schemes from [30] in capturing discontinuous solution (containing shocks and contact

waves) in essentially non-oscillatory manner and resolving fine-scale structures in a high speed shear instability flows.

2 Fifth-Order A-WENO Schemes: A Brief Description

We consider the 1-D system (1.1) on a certain interval covered with the uniform cells $[x_{j-\frac12}, x_{j+\frac12}]$ of size Δx centered at $x_j = (x_{j-\frac12} + x_{j+\frac12})/2$. Assuming that at a certain time t the point values $\boldsymbol{U}_j(t) \approx \boldsymbol{U}(x_j, t)$ are available (from now on we will omit the time dependence of all of the indexed quantities for the sake of brevity). These point values are then evolved in time according to the following semi-discretization:

$$\frac{\mathrm{d}}{\mathrm{d}t}\boldsymbol{U}_j = -\frac{\boldsymbol{\mathcal{F}}_{j+\frac12} - \boldsymbol{\mathcal{F}}_{j-\frac12}}{\Delta x}, \tag{2.1}$$

where $\boldsymbol{\mathcal{F}}_{j+\frac12}$ are numerical fluxes, which will be fifth-order accurate (see [11, 22, 31]) if we use the sixth-order accurate Taylor expansion of $\boldsymbol{\mathcal{F}}(x)$ at $x = x_{j+\frac12}$ (see [29]), namely, if

$$\boldsymbol{\mathcal{F}}_{j+\frac12} = \boldsymbol{\mathcal{F}}^{\mathrm{FV}}_{j+\frac12} - \frac{1}{24}(\Delta x)^2(\boldsymbol{F}_{xx})_{j+\frac12} + \frac{7}{5760}(\Delta x)^4(\boldsymbol{F}_{xxxx})_{j+\frac12}. \tag{2.2}$$

Here, $\boldsymbol{\mathcal{F}}^{\mathrm{FV}}_{j+\frac12}$ is the finite-volume numerical flux, taken to be the 1-D CURH numerical flux from [4, §2], which is a function of the left- and right-sided point values of $\boldsymbol{U}$ at $x = x_{j+\frac12}$. These one-sided point values, denoted by $\boldsymbol{U}^-_{j+\frac12}$ and $\boldsymbol{U}^+_{j+\frac12}$, respectively, are obtained using the WENO polynomial interpolation procedure with the Z-type weights (WENO-Z), applied in a characteristic-wise manner using the local characteristic decomposition [11, 22, 31]; also see the description provided in [30, §2.1]. The approximations of the second and fourth derivatives of the flux $\boldsymbol{F}$ on the right-hand side of (2.2) are computed using the standard central finite differences:

$$\begin{aligned}
(\boldsymbol{F}_{xx})_{j+\frac12} &= \frac{1}{48(\Delta x)^2}\left(-5\boldsymbol{F}_{j-2} + 39\boldsymbol{F}_{j-1} - 34\boldsymbol{F}_j - 34\boldsymbol{F}_{j+1} + 39\boldsymbol{F}_{j+2} - 5\boldsymbol{F}_{j+3}\right),\\
(\boldsymbol{F}_{xxxx})_{j+\frac12} &= \frac{1}{2(\Delta x)^4}\left(\boldsymbol{F}_{j-2} - 3\boldsymbol{F}_{j-1} + 2\boldsymbol{F}_j + 2\boldsymbol{F}_{j+1} - 3\boldsymbol{F}_{j+2} + \boldsymbol{F}_{j+3}\right),
\end{aligned} \tag{2.3}$$

where $\boldsymbol{F}_j := \boldsymbol{F}(\boldsymbol{U}_j)$.

Remark 2.1 The semi-discrete A-WENO scheme results in the system of time-dependent ODEs (2.1), which should be integrated by a sufficiently accurate, efficient and stable ODE solver. In the numerical experiments reported in §3, we have used the three stages third-order strong stability preserving (SSP) Runge-Kutta method; see, e.g., [7, 8]. The time steps have been chosen adaptively using the CFL number 0.45.

Remark 2.2 The proposed A-WENO scheme (2.1)–(2.3) can be extended to hyperbolic systems of balance laws,

$$\boldsymbol{U}_t + \boldsymbol{F}(\boldsymbol{U})_x = \boldsymbol{S}(\boldsymbol{U}),$$

in a straightforward way:

$$\frac{\mathrm{d}}{\mathrm{d}t}\boldsymbol{U}_j = -\frac{\boldsymbol{\mathcal{F}}_{j+\frac{1}{2}} - \boldsymbol{\mathcal{F}}_{j-\frac{1}{2}}}{\Delta x} + \boldsymbol{S}(\boldsymbol{U}_j),$$

where the numerical fluxes $\boldsymbol{\mathcal{F}}_{j+\frac{1}{2}}$ are still given by (2.2) and (2.3).

Remark 2.3 The 2-D extension of the described A-WENO scheme is performed in the dimension-by-dimension manner. We use the ND switch and the 2-D CURH numerical fluxes for the 2-D Euler equations of gas dynamics,

$$\begin{aligned}
&\rho_t + (\rho u)_x + (\rho v)_y = 0,\\
&(\rho u)_t + (\rho u^2 + p)_x + (\rho uv)_y = 0,\\
&(\rho v)_t + (\rho uv)_x + (\rho v^2 + p)_y = 0,\\
&E_t + \big[u(E+p)\big]_x + \big[v(E+p)\big]_y = 0.
\end{aligned} \tag{2.4}$$

are those presented in [4, §3]. In (2.4), ρ is the density, u and v are the x- and y-velocities, respectively, p is the pressure, and E is the total energy related to the other thermodynamic quantities through the equation of state, which for an ideal gas reads as

$$E = \frac{p}{\gamma - 1} + \frac{\rho}{2}(u^2 + v^2), \tag{2.5}$$

where γ is the specific heat ratio.

3 Numerical Examples

In this section, we present a variety of 1-D and 2-D numerical examples. The numerical results obtained by the proposed A-WENO schemes will be compared with the results computed by the A-WENO scheme recently proposed in [30]. For the sake of brevity, we will refer to these two schemes as the "NEW scheme" and the "OLD scheme", respectively. Our goal is to demonstrate that the NEW scheme leads to a higher resolution of contact waves, shear layers, vortices as well as large-scale 2-D structures. In Examples 1–6, we take $\gamma = 1.4$, while in Example 7, $\gamma = 5/3$.

3.1 One-Dimensional Examples

We first apply the NEW and OLD A-WENO schemes to the 1-D Euler equations of gas dynamics:

$$\begin{aligned}
&\rho_t + (\rho u)_x = 0,\\
&(\rho u)_t + (\rho u^2 + p)_x = 0,\\
&E_t + [u(E+p)]_x = 0,
\end{aligned}$$

where ρ is the density, u is the velocity, p is the pressure, and E is the total energy satisfying the following equation of states:

$$E = \frac{p}{\gamma - 1} + \frac{\rho u^2}{2}.$$

We have tested many 1-D benchmark examples including the slowly moving isolated contact discontinuity problem, the Lax problem, the shock-density wave interaction problem and the blast wave problem. The obtained results (most of which are not reported here for the sake of brevity) clearly indicate that the proposed NEW scheme is as robust as the OLD scheme. Since the ND switch is built for the 2-D system of equations only, in most of the 1-D examples we could not, as expected, observe any significant differences between the results computed by the NEW and OLD schemes as the tangential component of the velocity does not exist in the 1-D case. In Example 1 below, we present the computations for one specific example—the Blast wave problem, in which the NEW scheme slightly outperforms the OLD one.

Example 1—Blast Wave Problem

In the first example, we consider the following initial conditions:

$$(\rho(x,0),u(x,0),p(x,0))=\begin{cases}(1,0,1000), & x<0.1,\\ (1,0,0.01), & 0.1\geq x\leq 0.9,\\ (1,0,100), & x>0.9,\end{cases}$$

which are prescribed on the interval $[0,1]$, at both ends of which the solid wall boundary conditions are imposed. We compute the numerical solutions by both the NEW and OLD schemes until the final time $t=0.038$ on a uniform grid with $\Delta x=1/400$. The obtained densities are presented in Figure 3.1. From the local magnification subplots, one can see that the NEW scheme achieves a slightly better resolution than the OLD one.

3.2 Two-Dimensional Examples

We now turn to several 2-D examples for the compressible Euler equations (2.4) and (2.5).

Example 2—Double Mach Reflection

We first consider the double Mach reflection problem of a strong shock from an oblique surface, which is taken from [32]; also studied in [30]. The computational domain is $\Omega=[0,4]\times[0,1]$ and the initial data are given by

$$\big(\rho(x,y,0),u(x,y,0),v(x,y,0),p(x,y,0)\big)=\begin{cases}(8,8.25\cos\theta,-8.25\sin\theta,116.5), & x<\dfrac{1}{6}+\dfrac{y}{\sqrt{3}},\\ (1.4,0,0,1), & \text{otherwise},\end{cases}$$

where $\theta=\pi/6$. At $x=0$ and at the short part of the lower boundary $y=0$ in the interval $x\in[0,1/6]$, supersonic inflow boundary conditions are specified. At $x=4$, we impose the free-stream outflow boundary conditions. In the remaining part of the lower boundary, we use the solid wall boundary conditions, while at the upper boundary $y=1$, the exact solution of the Mach 10 moving oblique shock is imposed.

We compute the solutions until the final time $t=0.2$ on the uniform grid with $\Delta x=\Delta y=1/480$. The densities computed by the NEW and OLD schemes are shown in Figure 3.2. As one can see, both the NEW and OLD schemes can capture the following phenomena. First, the wall jet curl into a vortex occurs as the jet reaches the Mach stem. Furthermore, the shock that

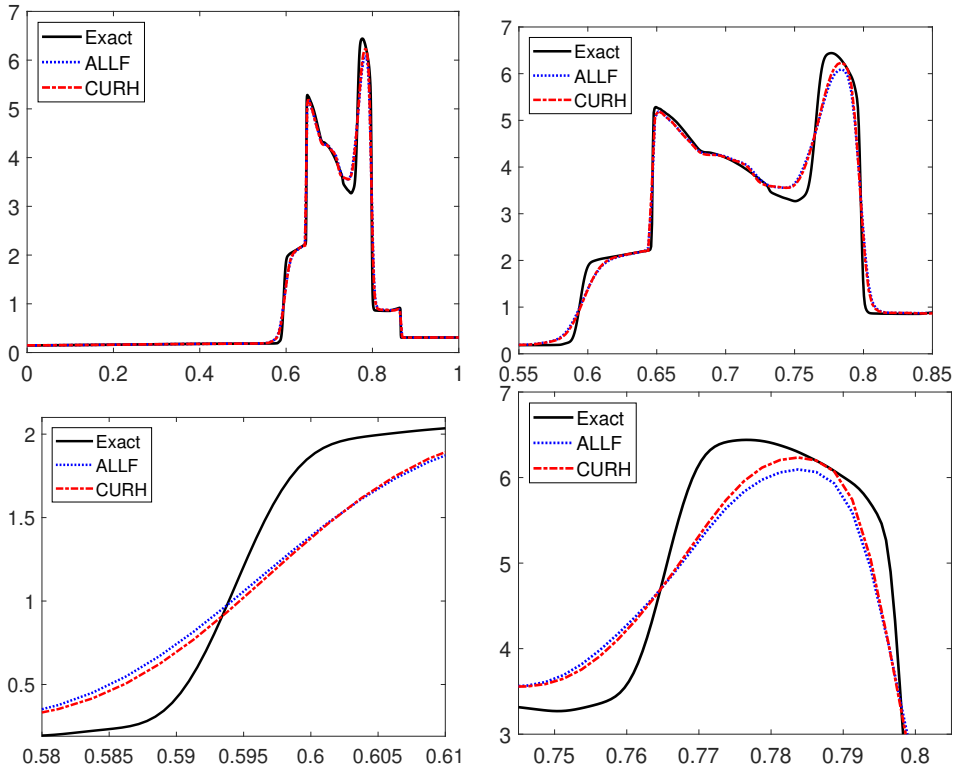

Figure 3.1: Example 1: Density (ρ) computed using both the NEW and OLD schemes (top left) together with the zooms at three different regions (top right and bottom row). The reference solution has been computed using the OLD scheme with $\Delta x = 1/3200$.

joins the contact surface and transverse wave (making this a double Mach reflection) sharpens and its triple point, the kink along the transverse wave, becomes much more distinguished. Finally, the Kelvin-Helmholtz (KH) instabilities along the contact surface, which grow through to the wall jet, are developed. It is clear that the NEW scheme captures these phenomena much better than the OLD scheme. Moreover, from Figure 3.3, where we zoom at the local structures at the tip of the jet, we can clearly see that the mushroom shape structures captured by the NEW scheme are slightly more curlier than those computed by the OLD scheme.

Example 3—Two-Dimensional Riemann Problem

In this example, we consider Configuration 3 of the 2-D Riemann problems from [18]; see also [26, 27, 33]. The initial conditions,

$$(\rho(x,y,0),u(x,y,0),v(x,y,0),p(x,y,0)) = \begin{cases} (1.5,0,0,1.5), & x>0.8,\ y>0.8,\\ (0.5323,1.206,0,0.3), & x<0.8,\ y>0.8,\\ (0.138,1.206,1.206,0.029), & x<0.8,\ y<0.8,\\ (0.5323,0,1.206,0.3), & x>0.8,\ y<0.8, \end{cases}$$

are prescribed in the computational domain $[0,1]\times[0,1]$ and supplemented with the free boundary conditions.

In Figure 3.4, we plot the densities computed by the NEW and OLD schemes on a uniform grid with $\Delta x = \Delta y = 1/400$ at the final time $t = 0.8$. As one can see, the NEW scheme can

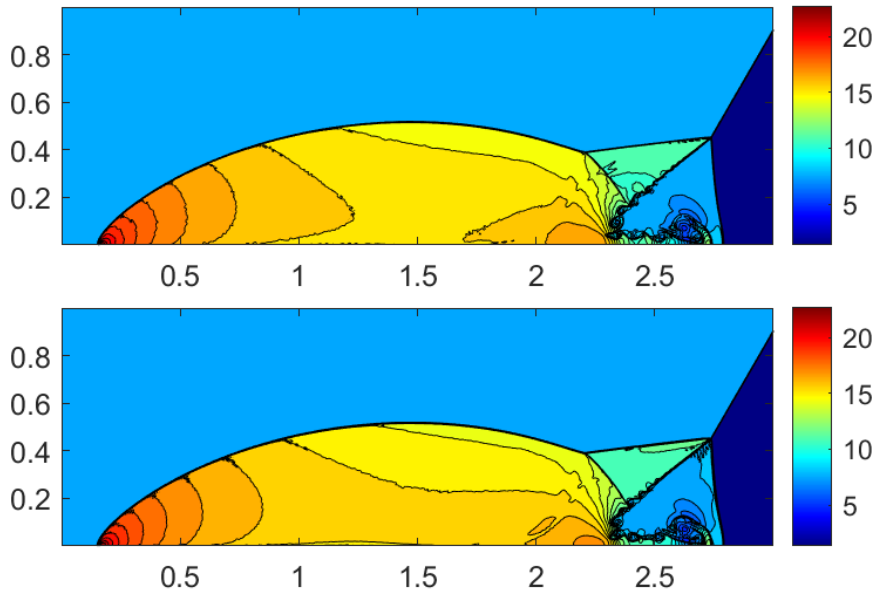

Figure 3.2: Example 2: Density (ρ) computed by the NEW (top) and OLD (bottom) schemes.

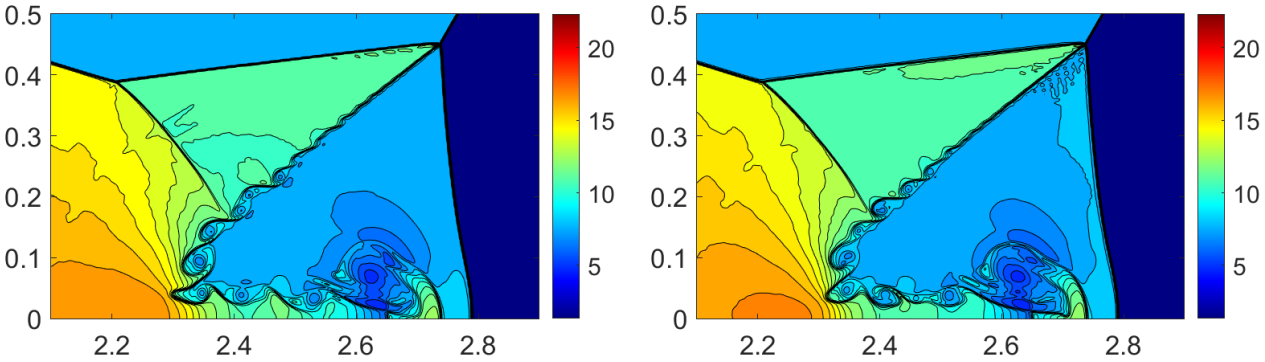

Figure 3.3: Same as in Figure 3.2, but zoom at the tip of the jet.

better capture a sideband instability of the jet in the zones of strong along-jet velocity shear and the instability along the jet's neck.

Example 4—Explosion Problem

In this example, we consider the explosion problem taken from [21] and also studied in [4, 14, 15, 17]. This is a circularly symmetric problem with an initial circular region of higher density and pressure:

$$\big(\rho(x,y,0),u(x,y,0),v(x,y,0),p(x,y,0)\big)=\begin{cases}(1,0,0,1), & x^2+y^2<0.16,\\ (0.125,0,0,0.1), & \text{otherwise.}\end{cases}$$

In this problem, the contact line develops instabilities as it is sensitive to perturbations of the initially circular interface represented by the discrete data on a Cartesian grid. Therefore, we use this example to compare the ND of different schemes.

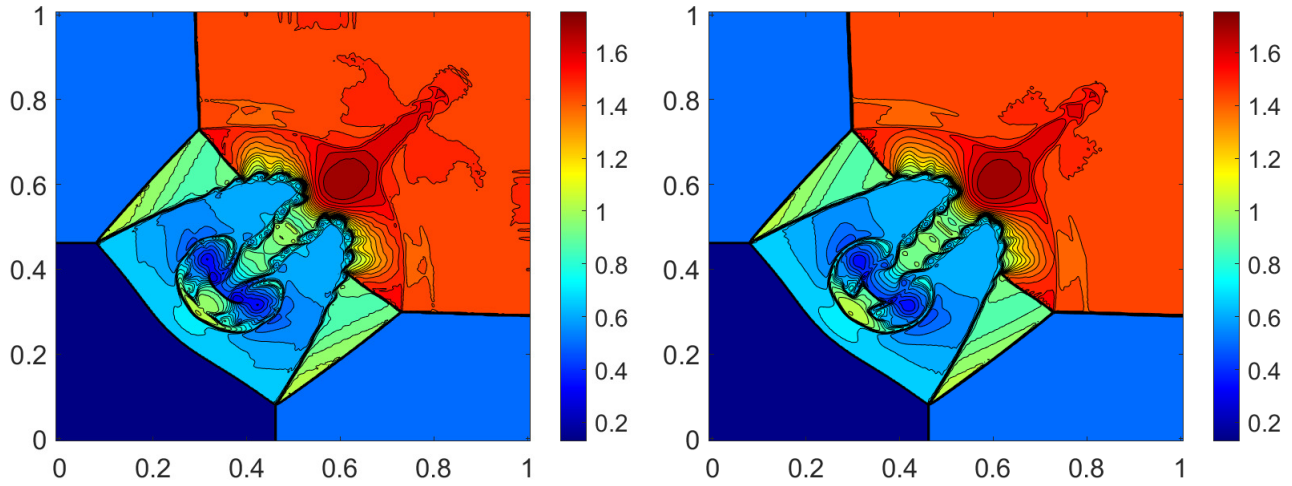

Figure 3.4: Example 3: Density (ρ) computed by the NEW (left) and OLD (right) schemes.

We compute the solution in the first quadrant $(x, y) \in [0, 1.5] \times [0, 1.5]$ using the uniform mesh with $\Delta x = \Delta y = 3/800$. Solid wall boundary conditions are imposed at $x = 0$ and $y = 0$, while free boundary conditions are set at $x = 1.5$ and $y = 1.5$. The densities computed by both the NEW and OLD schemes at the final time $t = 3.2$ are plotted in Figure 3.5. As expected, the contact curve captured by the NEW scheme is much "curlier" and the mixing layer is slightly "wider", and thus the contact wave part of the solution is more unstable than that captured by the OLD scheme. This indicates the lower ND of the NEW scheme as the contact curve is supposed to be unstable and may be stabilized by the ND only.

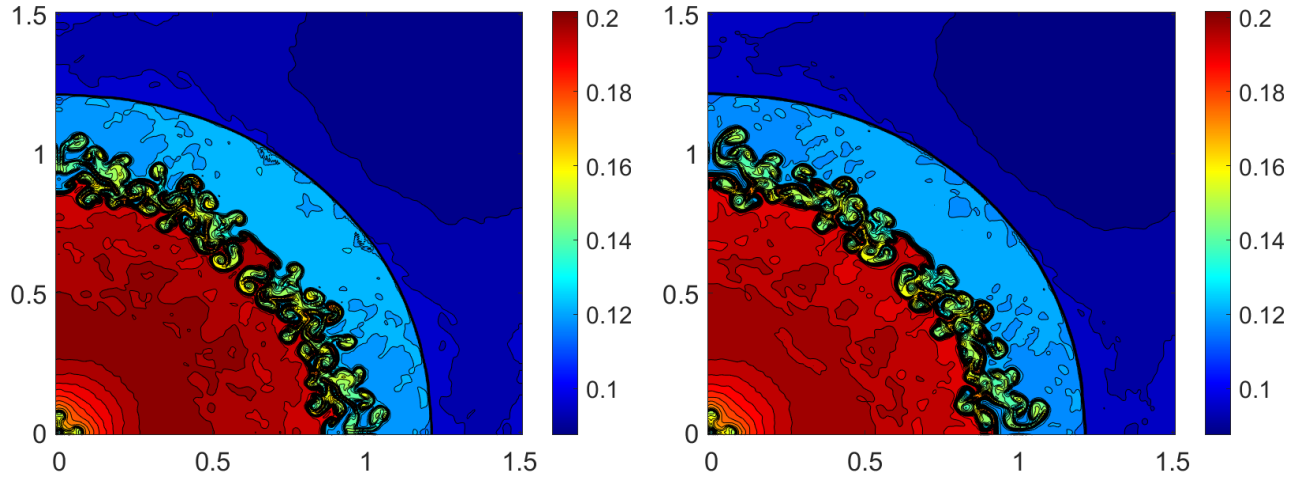

Figure 3.5: Example 4: Density (ρ) computed by the NEW (left) and OLD (right) schemes.

Example 5—Implosion Problem

In this example, we consider the implosion problem, which is a converging shock problem, which was studied in [4, 14, 15, 17, 21]. The computational domain is $[0, 0.3] \times [0, 0.3]$ and the initial

conditions are

$$\big(\rho(x,y,0),u(x,y,0),v(x,y,0),p(x,y,0)\big)=\begin{cases}(0.125,0,0,0.14), & |x|+|y|<0.15,\\ (1,0,0,1), & \text{otherwise},\end{cases}$$

so that the initial density and pressure are smaller inside the triangle than in the rest of the computational domain. Solid wall boundary conditions are imposed on all of the four boundaries.

We compute the solutions using both the NEW and OLD schemes until the final time $t=2.5$ on the uniform mesh with $\Delta x=\Delta y=3/4000$. The obtained ρ-components of the obtained numerical solutions are plotted in Figure 3.6. As one can see, a jet has formed in the results computed by both schemes. However, we observe that the jet generated by the NEW scheme propagates further in the direction of $y=x$ than the jet produced by the OLD one: This indicates a lower amount of the ND present in the NEW scheme.

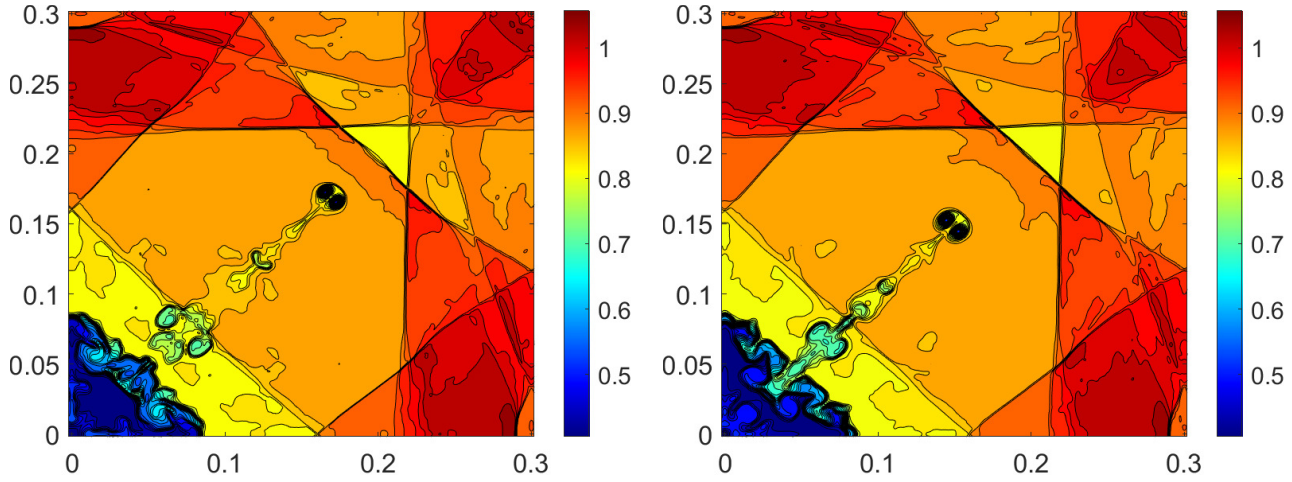

Figure 3.6: Example 5: Density (ρ) computed by the NEW (left) and OLD (right) schemes.

Example 6—Kelvin-Helmholtz (KH) instability

In this example, we study the KH instability, which frequently occurs in nature: two of its manifestations are the so-called "wind-over-water" and "clear air turbulence" instabilities. The KH instability is triggered by shear flows, often also involving fluids with different densities, and grows exponentially until the primary billows break, subsequently leading to a turbulent mixing of the two phases. In order to use the KH instability as a high-resolution test for the NEW scheme's capabilities of capturing small scale turbulent structures, we consider the following initial conditions [3, 4, 15, 24]:

$$\big(\rho(x,y,0),u(x,y,0)\big)=\begin{cases}\big(1,-0.5+0.5e^{(y+0.25)/L}\big), & y\in[-0.5,-0.25),\\ \big(2,0.5-0.5e^{(-y-0.25)/L}\big), & y\in[-0.25,0),\\ \big(2,0.5-0.5e^{(y-0.25)/L}\big), & y\in[0,0.25),\\ \big(1,-0.5+0.5e^{(0.25-y)/L}\big), & y\in[0.25,0.5],\end{cases}$$

$$v(x,y,0)=0.01\sin(4\pi x),\quad p(x,y,0)\equiv 1.5,$$

where L is a smoothing parameter (we take $L = 0.00625$), which corresponds to a thin shear interface with a perturbed vertical velocity field v in the conducted simulations. We expect that the difference between the initial fluid velocities across the interface will destabilize it. This will lead to the formation of KH vortices along the interface.

The computational domain is $[-0.5, 0.5] \times [-0.5, 0.5]$. We use a uniform grid with $\Delta x = \Delta y = 1/400$ and the periodic boundary conditions to compute the solutions by the NEW and OLD schemes until the final time $t = 4$. The densities obtained at times $t = 1$, 2.5 and 4 are plotted in Figure 3.7. As one can see, at the early time $t = 1$, the vortex streets formed by the NEW scheme are more pronounced. These structures continue growing exponentially in time and the most obvious difference in the performance of the two studied schemes is in the formation of "swirls", much more complicated vortices and the turbulent mixing of the two phases. This can be observed at later times $t = 2.5$ and 4, which confirms that the NEW scheme can capture the KH instabilities better than the OLD one.

Example 7—Raleigh-Taylor (RT) Instability

In the final example, we investigate the RT instability, which is a physical phenomenon occurring when a layer of heavier fluid is placed on top of a layer of lighter fluid. The RT instability phenomenon is important in many natural and industrial systems, such as supernova explosions, turbulent mixing and many others.

In order to study RT instabilities, we include a gravitational source term in the vertical momentum and energy equations. Assuming that the gravitation acts upward in the y-direction and setting the gravitational constant to be 1, we modify the 2-D Euler equations (2.4) as follows:

$$\begin{aligned}
&\rho_t + (\rho u)_x + (\rho v)_y = 0,\\
&(\rho u)_t + (\rho u^2 + p)_x + (\rho uv)_y = 0,\\
&(\rho v)_t + (\rho uv)_x + (\rho v^2 + p)_y = \rho,\\
&E_t + [u(E + p)]_x + [v(E + p)]_y = \rho v.
\end{aligned}$$

We use the setting from [28] (also see [4,15,30]) and consider the following initial conditions:

$$\big(\rho(x,y,0), u(x,y,0), v(x,y,0), p(x,y,0)\big) = \begin{cases} (2, 0, -0.025\,c\cos(8\pi x), 2y + 1), & y < 0.5,\\ (1, 0, -0.025\,c\cos(8\pi x), y + 1.5), & \text{otherwise,}\end{cases}$$

where $c := \sqrt{\gamma p/\rho}$ is the speed of sound. The computational domain is $[0, 1/4] \times [0, 1]$. We impose the solid wall boundary conditions at $x = 0$ and $x = 1/4$ and the Dirichlet boundary conditions at the top and bottom boundaries,

$$(\rho, u, v, p)\Big|_{y=1} \equiv (1, 0, 0, 2.5) \quad \text{and} \quad (\rho, u, v, p)\Big|_{y=0} \equiv (2, 0, 0, 1),$$

respectively.

We compute the numerical solutions by both the NEW and OLD schemes until the final time $t = 2.95$ using a uniform mesh with $\Delta x = \Delta y = 1/800$. In Figure 3.8, we plot the densities obtained at times $t = 1.95$ and 2.95. Due to the gravity in the system, the fluid with a higher density intruded into the fluid with a lower density. The initial velocity $v(x, y, 0)$ is not 0, but a cosine wave with small amplitude, which develops into a mushroom-like vortical structure due

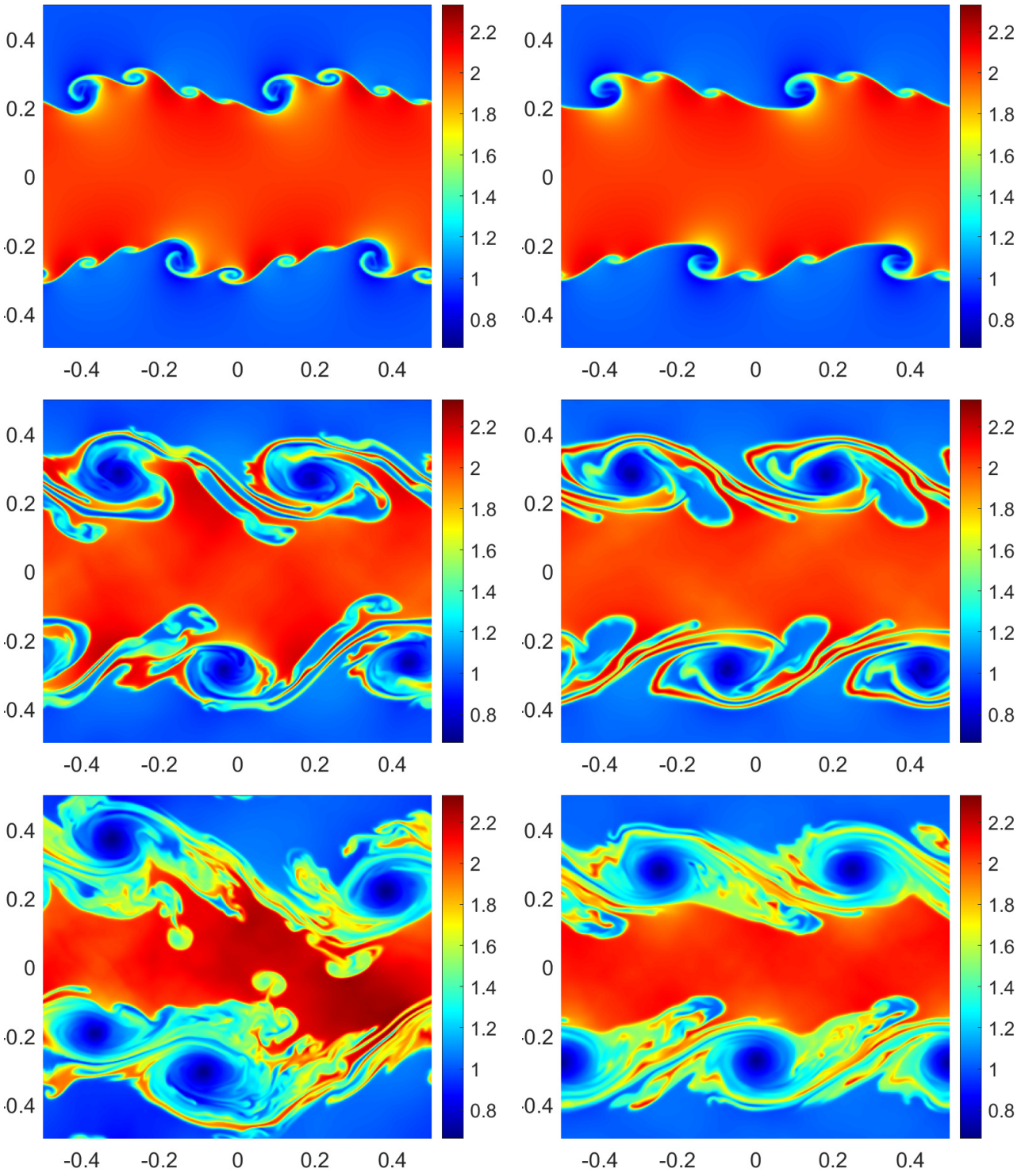

Figure 3.7: Example 6: Time snapshots of density (ρ) computed by the NEW (left column) and OLD (right column) schemes at $t = 1$ (top row), $t = 2.5$ (middle row) and $t = 4$ (bottom row).

to the vorticity generation with a nonalignment of the pressure gradient and density gradient (baroclinity) of a stratified fluid. The vortical structure in the simulation of the RT instability later develops into narrow trails. At earlier time $t = 1.95$, from the results obtained by the

NEW scheme, one can observe the appearance of two horn-like small structures at the top of the mushroom-like shape. Meanwhile, we also see that two small mushroom-like structures have been developed. At later time $t = 2.95$, the difference between the results obtained by the NEW and OLD schemes is even more pronounced. We can clearly see that the NEW scheme produces a more jellyfish-like structure, where the head of this "jellyfish" is extremely clear. Moreover, the "tentacles" generated by the NEW scheme are more abundant. Therefore, we conclude that the NEW scheme achieves a much better resolution of the complicated solution structures, which again indicates that the NEW scheme is less dissipative than the OLD one.

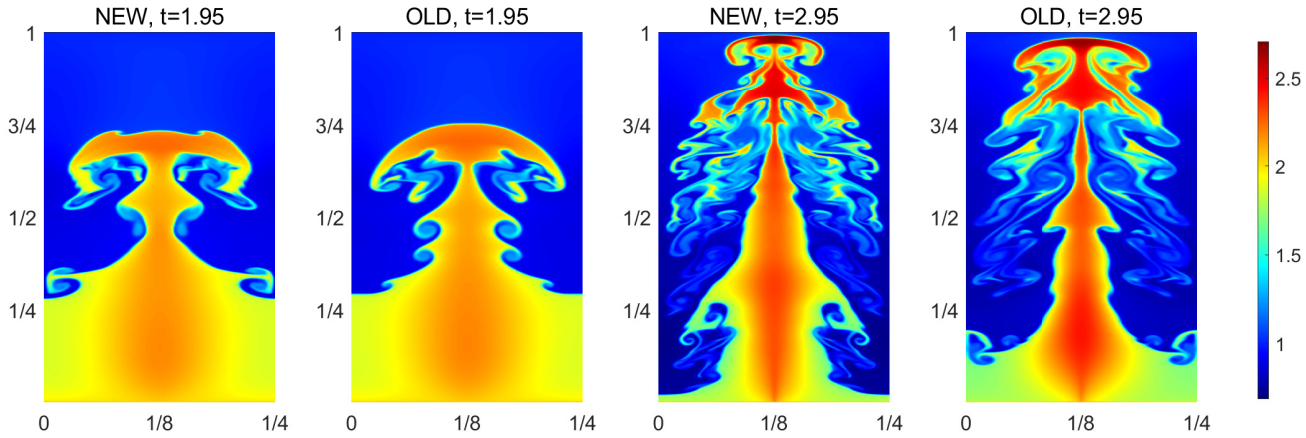

Figure 3.8: Example 7: Density (ρ) computed by the NEW and OLD schemes at times $t = 1.95$ and 2.95.

Acknowledgment: The work of B. S. Wang and W. S. Don was partially supported by the Ocean University of China through grant 201712011. The work of A. Kurganov was supported in part by NSFC grant 11771201 and by the fund of the Guangdong Provincial Key Laboratory of Computational Science and Material Design (No. 2019B030301001).

Conflict of Interest: On behalf of all authors, the corresponding author states that there is no conflict of interest.

References

[1] M. Ben-Artzi and J. Falcovitz, *Generalized Riemann problems in computational fluid dynamics*, vol. 11 of Cambridge Monographs on Applied and Computational Mathematics, Cambridge University Press, Cambridge, 2003.

[2] W. S. Don, D.-M. Li, Z. Gao, and B.-S. Wang, *A characteristic-wise alternative WENO-Z finite difference scheme for solving the compressible multicomponent non-reactive flows in the overestimated quasi-conservative form*, J. Sci. Comput., 82 (2020). Paper No. 27, 24 pp.

[3] U. S. Fjordholm, S. Mishra, and E. Tadmor, *On the computation of measure-valued solutions*, Acta Numer., 25 (2016), pp. 567–679.

[4] N. K. Garg, A. Kurganov, and Y. Liu, *Semi-discrete central-upwind Rankine-Hugoniot schemes for hyperbolic systems of conservation laws*, J. Comput. Phys., 428 (2021), p. 110078.

[5] N. K. Garg, S. V. Raghurama Rao, and M. Sekhar, *Weak-strong hyperbolic splitting for simulating conservation laws*, Int. J. Adv. Eng. Sci. Appl. Math., 7 (2015), pp. 62–69.

[6] E. Godlewski and P.-A. Raviart, *Numerical approximation of hyperbolic systems of conservation laws*, vol. 118 of Applied Mathematical Sciences, Springer-Verlag, New York, 1996.

[7] S. Gottlieb, D. Ketcheson, and C.-W. Shu, *Strong stability preserving Runge-Kutta and multistep time discretizations*, World Scientific Publishing Co. Pte. Ltd., Hackensack, NJ, 2011.

[8] S. Gottlieb, C.-W. Shu, and E. Tadmor, *Strong stability-preserving high-order time discretization methods*, SIAM Rev., 43 (2001), pp. 89–112.

[9] J. S. Hesthaven, *Numerical methods for conservation laws*, vol. 18 of Computational Science & Engineering, Society for Industrial and Applied Mathematics (SIAM), Philadelphia, PA, 2018. From analysis to algorithms.

[10] S. Jaisankar and S. V. Raghurama Rao, *A central Rankine-Hugoniot solver for hyperbolic conservation laws*, J. Comput. Phys., 228 (2009), pp. 770–798.

[11] Y. Jiang, C.-W. Shu, and M. Zhang, *An alternative formulation of finite difference weighted ENO schemes with Lax-Wendroff time discretization for conservation laws*, SIAM J. Sci. Comput., 35 (2013), pp. A1137–A1160.

[12] D. Kröner, *Numerical schemes for conservation laws*, Wiley-Teubner Series Advances in Numerical Mathematics, John Wiley & Sons Ltd., Chichester, 1997.

[13] A. Kurganov, *Central schemes: a powerful black-box solver for nonlinear hyperbolic PDEs*, in Handbook of numerical methods for hyperbolic problems, vol. 17 of Handb. Numer. Anal., Elsevier/North-Holland, Amsterdam, 2016, pp. 525–548.

[14] A. Kurganov and C.-T. Lin, *On the reduction of numerical dissipation in central-upwind schemes*, Commun. Comput. Phys., 2 (2007), pp. 141–163.

[15] A. Kurganov, Y. Liu, and V. Zeitlin, *Numerical dissipation switch for two-dimensional central-upwind schemes*. Submitted.

[16] ——, *Thermal vs isothermal rotating shallow water equations: comparison of dynamical processes in two models by simulations with a novel well-balanced central-upwind scheme*, Geophys. Astro. Fliud., (2020). To appear.

[17] A. Kurganov, M. Prugger, and T. Wu, *Second-order fully discrete central-upwind scheme for two-dimensional hyperbolic systems of conservation laws*, SIAM J. Sci. Comput., 39 (2017), pp. A947–A965.

[18] A. Kurganov and E. Tadmor, *Solution of two-dimensional riemann problems for gas dynamics without Riemann problem solvers*, Numer. Methods Partial Differential Equations, 18 (2002), pp. 584–608.

[19] R. J. LeVeque, *Finite volume methods for hyperbolic problems*, Cambridge Texts in Applied Mathematics, Cambridge University Press, Cambridge, 2002.

[20] P. Li, W. S. Don, and Z. Gao, *High order well-balanced finite difference WENO interpolation-based schemes for shallow water equations*, Comput. & Fluids, 201 (2020), p. 104476.

[21] R. Liska and B. Wendroff, *Comparison of several difference schemes on 1D and 2D test problems for the Euler equations*, SIAM J. Sci. Comput., 25 (2003), pp. 995–1017.

[22] H. Liu, *A numerical study of the performance of alternative weighted ENO methods based on various numerical fluxes for conservation law*, Appl. Math. Comput., 296 (2017), pp. 182–197.

[23] H. Liu and J. Qiu, *Finite difference Hermite WENO schemes for conservation laws, II: An alternative approach*, J. Sci. Comput., 66 (2016), pp. 598–624.

[24] J. Panuelos, J. Wadsley, and N. Kevlahan, *Low shear diffusion central schemes for particle methods*, J. Comput. Phys., 414 (2020), p. 109454.

[25] S. V. Raghurama Rao and K. Balakrishna, *An accurate shock capturing algorithm with a relaxation system for hyperbolic conservation laws*, in 16th AIAA Computational Fluid Dynamics Conference, 2003, p. 4115.

[26] C. W. Schulz-Rinne, *Classification of the Riemann problem for two-dimensional gas dynamics*, SIAM J. Math. Anal., 24 (1993), pp. 76–88.

[27] C. W. Schulz-Rinne, J. P. Collins, and H. M. Glaz, *Numerical solution of the Riemann problem for two-dimensional gas dynamics*, SIAM J. Sci. Comput., 14 (1993), pp. 1394–1394.

[28] J. Shi, Y.-T. Zhang, and C.-W. Shu, *Resolution of high order WENO schemes for complicated flow structures*, J. Comput. Phys., 186 (2003), pp. 690–696.

[29] C.-W. Shu and S. Osher, *Efficient implementation of essentially non-oscillatory shock-capturing schemes*, J. Comput. Phys., 77 (1988), pp. 439–471.

[30] B.-S. Wang, W. S. Don, N. K. Garg, and A. Kurganov, *Fifth-order A-WENO finite-difference schemes based on a new adaptive diffusion central numerical flux*, SIAM J. Sci. Comput., 42 (2020), pp. A3932–A3956.

[31] B.-S. Wang, P. Li, Z. Gao, and W. S. Don, *An improved fifth order alternative WENO-Z finite difference scheme for hyperbolic conservation laws*, J. Comput. Phys., 374 (2018), pp. 469–477.

[32] P. Woodward and P. Colella, *The numerical solution of two-dimensional fluid flowwith strong shocks*, J. Comput. Phys., 54 (1988), pp. 115–173.

[33] Y. Zheng, *Systems of conservation laws*, Progress in Nonlinear Differential Equations and their Applications, 38, Birkhäuser Boston, Inc., Boston, MA, 2001. Two-dimensional Riemann problems.